J Mol Model (2008) 14:403–408
DOI 10.1007/s00894-008-0290-3

ORIGINAL PAPER

The mechanism and kinetics of decomposition of 5-aminotetrazole

Jian-Guo Zhang · Li-Na Feng · Shao-Wen Zhang · Tong-Lai Zhang · Hui-Hui Zheng

Received: 4 December 2007 / Accepted: 9 February 2008 / Published online: 11 March 2008

Abstract The pathway and ab initio direct kinetics of the decomposition 5-aminotetrazole (5-ATZ) to HN_3 and NH_2CN was investigated. Reactant, products and transition state were optimized with MP2 and B3LYP methods using 6–311G** and aug-cc-pVDZ basis sets. The intrinsic reaction coordinate curve of the reaction was calculated using the MP2 method with 6–311G** basis set. The energies were refined using CCSD(T)/6–311G**. Rate constants were evaluated by conventional transition-state theory (CVT) and canonical variational transition-state theory (TST), with tunneling effect over 300 to 2,500 K. The results indicated that the tunneling effect and the variational effect are small for the calculated rate constants. The fitted three-parameter expression calculated using the CVT and TST methods are $k(T) = 4.07 \times 10^{11} \times T^{0.84} \times e^{\left(-2.42\times10^4/T\right)} s^{-1}$ and $k(T) = 2.09 \times 10^{11} \times T^{0.89} \times e^{\left(-2.36\times10^4/T\right)} s^{-1}$, respectively.

Keywords 5-Aminotetrazole · Ab initio calculation · Transition state theory · Rate constant

Introduction

Tetrazoles have the highest nitrogen content of all organic substances, and exhibit surprisingly high thermal stability [1, 2]. Aminotetrazoles are prospective gas-generating materials and blowing agents for polymeric systems, because they are sufficiently stable thermally and yield a large volume of gas upon thermal decomposition. Among the aminotetrazoles, 5-aminotetrazole (5-ATZ), which is used as a gas generator and key intermediate in many organic syntheses [3], has received by far the most attention in the literature. In addition, it is often used as an environmentally friendly gas-generating material [4–8]. The synthesis of 5-ATZ, by reacting dicyandiamide and sodium azide in acid-catalyzed condition, was described as early as 1892 by Thiele [9]. The most direct method to form tetrazole is via the concerted and highly regioselective [2, 3] cycloaddition between HN_3 and NH_2CN [10].

Since 5-ATZ is widely used in the field of energetic materials (such as gas-generating materials), it seemed important to investigate the mechanism and kinetics of its thermal decomposition. Brill [11, 12] and Ivashkevich et al. [13–18] studied the thermal decomposition process and kinetics of an ATZ series of compounds using thermogravimetry (TG), thermal volumetric analysis (TVA), evolved gas analysis (EGA) and other related thermal analysis methods. The mechanism of decomposition of ATZ is complex, and may consist of several fundamental steps, but such experiments have shown that HN_3 and NH_2CN are the initially detected products [19]. It is currently accepted that the mechanism of the initial decomposition process of 5-ATZ proceeds via the mechanism shown in Fig. 1. However, to the best of our knowledge, both energetic information and kinetic data for the decomposition of 5-ATZ are quite limited, which has attracted the interest of experimental chemists [19, 20]. As for any theoretical investigation, we found no closely related reference except that of Chen [21], who studied the synthetic reaction of tetrazole and tetrazolate anion using theoretical calculation methods.

J.-G. Zhang (✉) · L.-N. Feng · T.-L. Zhang · H.-H. Zheng
State Key Laboratory of Explosion Science and Technology,
Beijing Institute of Technology,
Beijing 100081, P. R. China
e-mail: zhangjianguobit@yahoo.com.cn

S.-W. Zhang
School of Science, Beijing Institute of Technology,
Beijing 100081, P. R. China

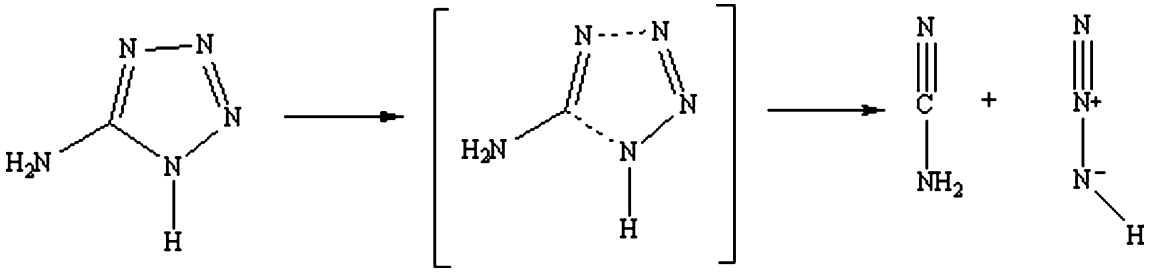

Fig. 1 The mechanism of the decomposition process of 5-aminotetrazole (5-ATZ) to HN_3 and NH_2CN

Here, we present a kinetic study of the decomposition of 5-ATZ by employing a direct ab initio kinetics method. In our experience, values calculated using the MP2 method are closer to experiment data; also, B3LYP is a popular and economical method. So, in this paper, the reactant, products, and transition state (TS) have been fully optimized using the MP2 [22, 23] and B3LYP methods [24, 25] with 6–311G** [26-28] and aug-cc-pVDZ basis sets [29-31]. The intrinsic reaction coordinate (IRC) curve of reactions is calculated using MP2/6–311G** level of theory. Rate constants are calculated using the canonical variational transition-state theory (CVT) and transition-state theory (TST) theory with small curvature tunneling correction and Eckart correction.

Computational methods

Electronic structure calculations

Geometries and frequencies of all stationary points (reactant, product, and TS) were optimized using the MP2 and B3LYP methods with the 6–311G**, aug-cc-pVDZ basis sets. Here, MP2 stands for the second-order Møller-Plesset (many-body) perturbation theory, B3LYP is a DFT method using Becke's three-parameter nonlocal exchange functional with the nonlocal correlation of Lee, Yang, and Parr. The 6–311G** is a split-valence triple-zeta plus polarization basis set [26–28], and cc-pVDZ expresses Dunning's correlation functional consistent polarized valence double-zeta basis sets [29, 30]. When the aug- prefix is used to add diffuse functions to the cc-pVDZ basis sets, one diffuse function of each function type is used for each given atom added [31]. aug-cc-pVDZ is an abbreviation for Dunning's augmented, correlation-consistent, polarized-valence double-basis set. To yield more reliable values for reaction enthalpy and barrier, the energies of all stationary points were further refined with several multi-level methods such as the CCSD (T) and QCISD (T) methods with the 6–311G** basis set. Here CCSD (T) stands for a couple-cluster single- and double- substitution method with a perturbative treatment of triple excitations [32]. QCISD calculates a quadratic CI (with single and double excitations) energy. QCISD(quadratic configuration interaction with single and double substitutions) gives a perturbative estimate of the effects of triple excitations.. The reactants and products are refined with G3 [33], G3MP2 [34], CBS-QB//3 [35]. The minimum energy path (MEP) is obtained using the intrinsic reaction coordinate (IRC) method [36] at the MP2/6–311G** level of theory. In the calculation of rate constants, the single-point energy calculation for the stationary points and a few extra points along the MEP were refined to establish the electronic potential curve at the CCSD(T)/6–311G** level of theory. All the electronic structure calculations were carried out in our laboratory using the program GAUSSIAN 03 [37].

Rate constant calculations

Calculations of reaction kinetics were carried out on the basis of initial information (optimized geometries, energies, gradients, and frequencies along the MEP). In general, the tunneling effect of the reaction in which hydrogen takes part will be obvious. According to this rule, the tunneling effect should be inconspicuous for our calculated system. To test the system, we chose different methods to calculate the rate constant. Rate constants were evaluated using the conventional transition-state theory (TST) [38], the canonical variational transition-state theory (CVT) [39–41], CVT with small curvature tunneling correction (CVT/SCT) [42, 43], and TST rate constant calculations with Eckart tunneling correction (TST/Eckart) [44] by employing the online Vklab program package [45] and POLYRATE 8.2 program [46] over a wide temperature region from 200 to 2,500 K. Tunneling is included by the SCT correction. Within the framework of CVT, the generalized transition state constant, $k^{GT}(T, s)$ can be calculated at the reaction coordinate*s* along the MEP at a fixed temperature; CVT rate constants are then obtained by minimizing $k^{GT}(T, s)$ along the MEP at the given temperature as follows:

$$k^{cvt}(T) = \min_{s} k^{GT}(T, s)$$

Here "*s*" is the reaction coordinate, $k^{GT}(T, s)$ is the rate constant of generalized TST rate constant at the dividing surface that intersects the MEP at *s* and is orthogonal to the

MEP at the intersection point. The CVT rate constants are corrected with the SCT transmission coefficient.

Results and discussion

Geometries and energies

The optimized structures for the reactants, products and TS at the MP2/6–311G** level of theory are given in Fig. 2. The optimized geometric parameters for the reactants, products and TS using the MP2 and B3LYP method with 6–311G** and aug-cc-pVDZ levels along with available experimental values are given in Table 1. The optimized geometrical parameters of 5-ATZ at all levels of theory employed are in agreement with the available experimental values within the allowed error range. Thus, we can infer that our calculations are meaningful. On the other hand, as far as we know, 5-ATZ often exists as 5-aminotetrazole monohydrate, and some isomers of 5-ATZ coexist under certain experimental conditions, so experimental geometry data for 5-ATZ are quite limited. The harmonic vibrational frequencies were calculated to confirm the stationary nature of 5-ATZ and to make zero-point energy (ZPE) corrections. All of the minima, including reactants and products, possess only real frequencies, while the TS is confirmed by normal-mode analysis to have one, and only one, imaginary frequency corresponding to the stretching modes of the coupling between breaking and forming bonds.

Table 2 gives the harmonic vibrational frequencies and ZPEs of the equilibrium and TS structure of the reaction by the MP2 method at the 6–311G** level along with the available experimental data. The predicted values of the imaginary frequency for the reaction is 605*i* at MP2/6–311G** level of theory. The frequencies calculated within all the models are considered to agree with experimental data (taking into account experimental uncertainty) for all species. The calculated values of between 3,200 and 3,600 cm^{-1} are likely due to υ_{NH}. The values between 3,150 and 3,200 cm^{-1} are likely due to υ_{NH} of the tetrazole ring. The band at about 1,640 cm^{-1} is assigned to δ_{NH}, and that about 1,140 cm^{-1} to υ_{CN}. The values between 900 and 1,160 cm^{-1} are likely due to $\upsilon_{\text{tetrazole ring}}$. The values below 780 cm^{-1} are assigned to $\delta_{\text{NH rocking}}$.

Table 3 abstracts the reaction energies (ΔE), the classical potential barriers (V_{MEP}), ground-state vibrationally adiabatic energy curve (V_a^G), which is the refined energies calculated using CCSD(T)/6–311G** with ZPE at MP2/6–311G** level (V_{MEP}+ZEP), and the reaction enthalpies (ΔH^0_{298K}); we can see that all these values are relevant to the methods and basis sets employed. Generally, all the values become smaller as the theory and basis sets became higher and larger, respectively. So, combined multi-level methods are required to obtain good estimations of related energetic values. In the calculation of the V_a^G of QCISD(T)/6–311G** and CCSD(T)/6–311G** in Table 3, we take advantage of the ZPEs at MP2/6–311G** level. The largest values of ΔE, V_{MEP}, V_a^G and ΔH are 27.53, 52.58, 49.18 and 24.09 kcal mol^{-1} at B3LYP/aug-cc-pVDZ level of theory, respectively. The multi-level methods yield significant improvement on these energies and agree well with each other. We compared the results with data obtained experimentally. Although the experimental data [17] of ΔH^0_{298K} (28.03 kcal mol^{-1}) are larger than the calculated

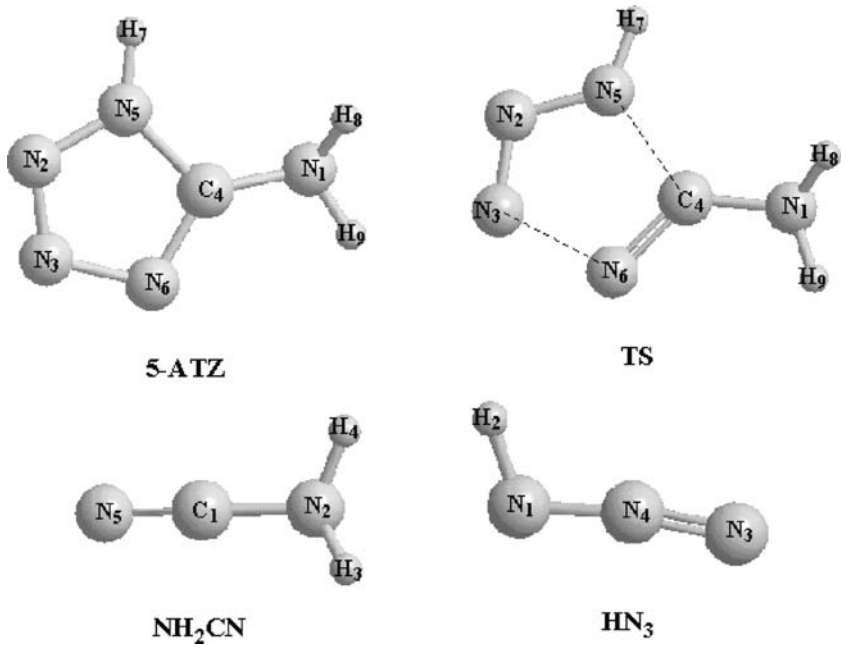

Fig. 2 Structure and atom number of stationary points, and the transition state (TS) for the reaction using MP2/6–311G**

Table 1 The optimized geometries of reactants, products and transition state (TS) at different levels of theory. *5-ATZ* 5-aminotetrazole

Species	Parameter	MP2/6–311G**	B3LYP/6–311G**	MP2/aug-cc-pVDZ	B3LYP/aug-cc-pVDZ	Experimental
5-ATZ	R(1,4)	1.387	1.374	1.394	1.370	
	R(2,3)	1.311	1.280	1.326	1.277	1.255[a]
	R(2,5)	1.349	1.368	1.355	1.365	1.373[a]
	R(3,6)	1.360	1.364	1.368	1.361	1.381[a]
	R(4,5)	1.351	1.350	1.357	1.346	
	R(4,6)	1.322	1.318	1.334	1.316	
	A(4,1,9)	109.4	112.0	109.6	112.9	
	A(3,2,5)	105.5	105.8	105.4	105. 9	
	A(2,3,6)	111.2	111.9	111.0	111.8	
	A(1,4,6)	127.4	126.3	127.4	126.2	
	A(5,4,6)	108.1	108.3	108.0	108.3	
	A(2,5,4)	109.2	108.2	109.5	108.2	
	A(3,6,4)	106.1	105.8	106.1	105.8	
TS	R(1,4)	1.380	1.364	1.384	1.361	
	R(2,3)	1.175	1.161	1.184	1.156	
	R(2,5)	1.300	1.280	1.307	1.276	
	R(3,6)	2.127	2.093	2.132	2.083	
	R(4,5)	1.797	1.920	1.825	1.923	
	R(4,6)	1.221	1.196	1.234	1.193	
	A(4,1,9)	111.9	113.3	112.7	113.8	
	A(3,2,5)	132.8	133.5	133.4	134.0	
	A(2,3,6)	95.8	96.9	96.0	96.8	
	A(1,4,5)	103.1	103.8	103.3	104.2	
	A(1,4,6)	142.1	147.2	142.1	147.2	
	A(5,4,6)	114.8	109.0	114.5	108.6	
	A(2,5,4)	99.5	98. 9	98.8	98.6	
	A(2,5,7)	110.2	113.2	109.7	113.5	
	A(3,6,4)	96.5	101.3	96.8	101.6	
NH_2CN	R(1,2)	1.356	1.342	1.363	1.340	
	R(1,5)	1.175	1.157	1.188	1.155	
	A(2,1,5)	176.8	177.4	176.2	177.3	
	A(1,2,3)	112.5	115.3	112.7	115.5	
	A(3,2,4)	111.5	113.5	111.2	113.5	
HN_3	R(1,4)	1.247	1.238	1.259	1.236	
	R(3,4)	1.151	1.131	1.161	1.125	
	A(2,1,4)	109.0	110.1	109.2	110.6	
	A(1,4,3)	171.0	171.5	170.3	171.7	

[a] From [17]

values, the latter seem to be consistent with the results of others, and the calculated values of ΔE are in good agreement with the experimental data [17, 19]. The deviation between calculated and experiment data may be due to the complications of 5-ATZ decomposition in an experimental setting, and experimental error should be taken into account.

Reaction and properties

Although the optimized geometric parameters under MP2/6–311G** were not very close to the experimental data, the latter were measured for the solid compound, taking into account the effect of the crystal lattice, but our calculated data refer to the gas state. MP2/6–311G** is currently considered more exact (and a reasonable compromise between expense and accuracy), MEPs being obtained using IRC theory at the MP2/6–311G** level of theory, with further refinement of potential energy profiles using CCSD(T)/6–311G** level. The IRC calculation predicts that HN_3 and NH_2CN are the products of the 5-ATZ decomposition reaction. Figure 3 depicts the vibrationally adiabatic ground-state potential energy curve (V_a^G) and the classical potential barriers (V_{MEP}) of the reaction as a function of *s*. The energies of the vibrationally adiabatic ground-state potential energy curve (V_a^G) used are the refined energies from the CCSD(T)/6–311G** method based on the ZPE at MP2/6–311G** level of theory, while the energies of the classical potential barriers (V_{MEP}) used

Table 2 Harmonic frequencies (cm^{-1}) and zero point energies (ZPE; kcal mol^{-1}) for the reactant, products and TS at MP2/6–311G**

Species		Harmonic frequencies	ZPE
5-ATZ	Calculated	216, 301, 384, 565, 693, 718, 731, 820, 1016, 1075, 1114, 1131, 1167, 1211, 1383, 1516, 1621, 1672, 3581, 3683, 3689	40.44
	Experimental[a]	740, 825, 1000, 1384, 3380, 3485	
TS	Calculated	605*i*, 195, 260, 375, 392, 498, 523, 575, 670, 741, 773, 1101, 1198, 1258, 1279, 1652, 1902, 2021, 3503, 3587, 3693	37.45
NH_2CN	Calculated	401, 469, 715, 1068, 1216, 1640, 2261, 3590, 3692	21.52
	Experimental	1585[b], 2264[c], 3497[d]	
HN_3	Calculated	543, 567, 1138, 1261, 2369, 3550	13.48
	Experimental	1138[b], 1265[d], 1282[b], 2310[b]	

[a] From [17]
[b] From [11]
[c] From [47]
[d] From [48]

are data from the CCSD(T)/6–311G** method. It can be seen that the curves are relatively smooth. This type of reaction is anticipated to have only a small tunneling effect.

Rate constant calculations

The rate constants of the decomposition products of 5-ATZ are calculated using the TST, TST/Eckart, CVT(T), CVT/ZCT and CVT/SCT methods with MEP refined from the CCSD(T)/6–311G** method based on the MP2/6–311G** level of theory. The rate constants are shown in Fig. 4. The rate constants calculated by TST and TST/ Eckart are almost identical over the whole temperature range. As discussed in the previous section, the MEP of the reaction is smooth and this may result in a small tunneling effect

Table 3 Reaction energetic parameters (kcal mol^{-1}) at different levels of theory. *MEP* Minimum energy path

	ΔE	V_{MEP}	V_a^G	ΔH
B3LYP/6–311G**	22.15	48.39	45.11	18.76
MP2/6–311G**	20.76	46.06	43.07	17.13
B3LYP/aug-cc-pVDZ	27.53	52.58	49.18	24.09
MP2/aug-cc-pVDZ	25.76	45.79	42.80	22.18
CCSD(T)/6–311G**	23.57	49.29	46.30	
QCISD(T)/6–311G**	22.96	48.85	45.87	
G3MP2B3	23.74			
CBS-Q//B3	23.47			
Experimental	21.51–32.27[a]			28.03[a]

[a] From [17]

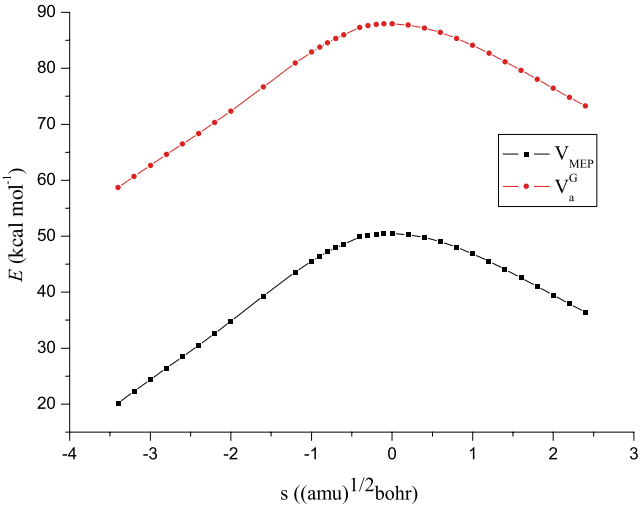

Fig. 3 The vibrationally adiabatic ground-state potential energy curve (V_a^G) and the classical potential barriers (V_{MEP}) of the reaction as a function of *s* $(amu)^{1/2}$ bohr at the MP2/6–311G** level of theory

over the whole temperature range. At the same time, from the CVT-calculated results, we find that the variational effect for the reaction is minimal. The rate from CVT is somewhat less than the value obtained from the TST method. In addition, the small-curvature tunneling (SCT) and zero-curvature tunneling (ZCT) transmission coefficients are inconspicuous. It can be seen that, at temperatures below 1,000 K, the rate constants of CVT/SCT are slightly larger than those of CVT. The rate constant calculation gives a good description of the decomposition of 5-ATZ. Since no direct hydrogen motion is included in the reaction, the tunneling effect is inconspicuous. The activation energy values obtained using the fitting method from TST, TST/Eckart, CVT, CVT/ZCT, and CVT/SCT are 46.83, 46.21, 48.15, 46.96, and 46.64 kcal mol^{-1}, respectively. These calculated data are

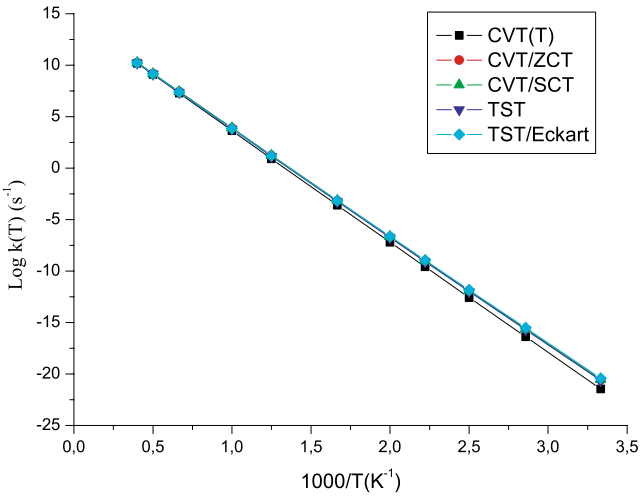

Fig. 4 Arrhenius plot of rate constants calculated at the TST, TST/Eckart, CVT, CVT/SCT and CVT/ZCT levels of theory. The rate constants are calculated based on the interpolated MEP at the MP2/6–311G** level of theory

consistent with the experimental value of 47.77 kcal mol^{-1} [19] for the initial decomposition of 5-ATZ from thermal analysis technologies. The fitted three-parameter expression calculated from the CVT and TST methods are $k(T) = 4.07 \times 10^{11} \times T^{0.84} \times e^{\left(-2.42\times10^4/T\right)} s^{-1}$ and $k(T) = 2.09 \times 10^{11} \times T^{0.89} \times e^{\left(-2.36\times10^4/T\right)} s^{-1}$, respectively. According to the calculated results, when 5-ATZ is used as a gas-generating material or blowing agent, the choice of an appropriate temperature will yield more gas production.

Summary

A direct study of the kinetics of the thermal rate constants of the decomposition of 5-ATZ was carried out using DFT and MP2 methods with 6–311G** and aug-cc-pVDZ basis sets. The geometries and harmonic vibrational frequencies of all stationary points were calculated by means of B3LYP and MP2 with 6–311G** and aug-cc-pVDZ basis sets. Information regarding the MEP was obtained at MP2/6–311G**. The energies and enthalpies are refined using CCSD(T)/6–311G** and QCCSD(T)/6–311G**. The rate constants of the reaction were calculated using the TST, TST/Eckart, CVT(T), CVT/ZCT and CVT/SCT methods. The calculated values of ΔE are in good agreement with the experimental data. The calculation results indicate that the tunneling effect and the variational effect for the calculated rate constants are small.

Acknowledgments The authors would like to thank Professor D.G. Truhlar for proving the POLYRATE 8.2 program. The project was supported by NSAF Foundation (No. 10776002) of the National Natural Science Foundation of China and Chinese Academy of Engineering Physics.

References

1. Levchik SV, Balabanovich AI, Ivashkevich OA, Gaponik PN, Costa L (1995) Polym Degrad Stability 47:333–338
2. Lesnikovich II, Sviridov VV, Printsev GV, Ivashkevich OA, Gaponik PN (1986) Nature 323:706–707
3. Katritzky AR, Rogovoy BV, Kovalenko KV (2003) J Org Chem 68:4941–4943
4. Baglini JL, Helmy AK, Stang PL, Dunkerson DE, Wright JH (2004) WO2004080921-A2
5. Mendenhall IV, Taylor RD (2006) US Patent 2006289096-A1
6. Taylor RD, Mendenhall IV (2006) WO2006047085-A2
7. Lund GK, Blau RJ (1996) US Patent 5,500,059
8. Ramaswamy CP, Grzelczyk C (1997) US Patent 5,661,261
9. Thiele J (1892) Liebigs Ann 270:54–63
10. Himo F, Demko ZP, Noodleman L, Sharpless KB (2003) J Am Chem Soc 125:9983–9987
11. Brill TB, Ramanathan H (2000) Combust Flame 122:165–171
12. Gao A, Oyumi Y, Brill TB (1991) Combust Flame 83:345–352
13. Lesnikovich AI, Ivashkevich OA, Printsev GV, Gaponik PN, Levchik SV (1990) Thermochim Acta 171:207–213
14. Lesnikovich AI, Levchik SV, Balabanovich AI, Ivashkevich OA, Gaponik PN (1992) Thermochim Acta 200:427–441
15. Reddy GO, Mohan VK, Murali BKM, Chatterjee AK (1981) Thermochim Acta 43:61–73
16. Vyazovkin SV, Lesnikovich AI, Lyutsko VA (1990) Thermochim Acta 165:17–22
17. Levchik SV, Ivashkevich OA, Balabanovich AI, Lesnikovich AI, Gaponik PN, Costa L (1992) Thermochim Acta 207:115–130
18. Lesnikovich AI, Printsev GV, Ivashkevich OA, Gaponik PN, Shandakov VA (1991) Thermochim Acta 184:221–231
19. Lesnikovich AI, Ivashkevich OA, Levchik SV, Balabanovich AI, Gaponik PN, Kulak AA (2002) Thermochim Acta 388:233–251
20. Brill TB, Ramanathan H (2000) Combust Flame 122:333–338
21. Chen C (2000) Int J Quantum Chem 80:27–37
22. Head-Gordon M, Pople JA, Frisch MJ (1988) Chem Phys Lett 153:503–509
23. Frisch MJ, Head-Gordon M, Pople JA (1990) Chem Phys Lett 166:281–289
24. Lee C, Yang W, Parr RG (1988) Phys Rev B 37:785–789
25. Becke AD (1993) J Chem Phys 98:5648–5652
26. Hehre WJ, Radom L, Schleyer PVR, Pople JA (1986) Ab initio molecular orbital theory. Wiley, New York
27. Krishnan R, Binkley JS, Seeger R, Pople JA (1980) J Chem Phys 72:650–677
28. Petersson GA, Bennett A, Tensfeldt TG, Al-Laham MA, Shirley WA, Mantzaris J (1988) J Chem Phys 89:2193–2197
29. Dunning TH Jr (1989) J Chem Phys 90:1007–1023
30. Kendall RA, Dunning TH Jr, Harrison RJ (1992) J Chem Phys 96:6796–6806
31. Woon DE, Dunning TH Jr (1993) J Chem Phys 98:1385–1393
32. Purvis GD, Bartlett RJ (1982) J Chem Phys 76:1910–1918
33. Curtiss LA, Raghavachari K, Redfern PC, Rassolv V, Pople JA (1998) J Chem Phys 109:7764–7776
34. Baboul AG, Curtiss LA, Redfern PC, Raghavachari K (1999) J Chem Phys 110:7650–7657
35. Montgomery JA, Frisch MJ, Ochterski JW, Petersson GA (2000) J Chem Phys 112:6532–6542
36. Gonzalez C, Schlegel HB (1989) J Chem Phys 90:2154–2161
37. Frisch MJ, Trucks GW, Schlegel HB, Scuseria GE, Robb MA, Cheeseman JR, Zakrzewski VG, Montgomery JA, Stratmann RE, Burant JC, Dapprich S, Millam JM, Daniels AD, Kudin KN, Strain MC, Farkas O, Tomasi J, Barone V, Cossi M, Cammi R, Mennucci B, Pomelli C, Adamo C, Clifford S, Ochterski J, Petersson GA, Ayala PY, Cui Q, Morokuma K, Malick DK, Rabuck AD, Raghavachari K, Foresman JB, Cioslowski J, Ortiz JV, Baboul AG, Stefanov BB, Liu G, Liashenko A, Piskorz P, Komaromi I, Gomperts R, Martin RL, Fox DJ, Keith T, Al-Laham MA, Peng CY, Nanayakkara A, Challacombe M, Gill PMW, Johnson B, Chen W, Wong MW, Andres JL, Gonzalez C, Head-Gordon M, Replogle ES, Pople JA (2003) Gaussian 03, Revision A.1. Gaussian Inc, Pittsburgh PA
38. Truhlar DG, Isaacson AD, Garrett BC (1985) Theory of chemical reaction dynamics, vol. 4, CRC Press, Boca Raton
39. Miller WH (1979) J Am Chem Soc 101:6810–6814
40. Truhlar DG, Garrett BC (1984) Annu Rev Phys Chem 35:159–189
41. Truong NT (1994) J Chem Phys 100:8014–8025
42. Liu YP, Lynch GC, Troung TN, Lu DH, Truhlar DG, Garrett BC (1993) J Am Chem Soc 115:2408–2415
43. Truhlar DG, Isaacson AD, Garrett BC (1982) J Phys Chem 86:2252–2263
44. Truong NT, Truhlar DG (1990) J Chem Phys 93:1761–1769
45. Zhang SW, Truong TN (2001) VKLab version 1.0, University of Utah
46. Chuang YY, Corchado JC, Fast PL, Will J, Hu WP, Liu YP, Lynch GC, Jackels CF, Nguyen KA, Gu MZ, Rossi I, Isaacson EL, Truhlar DG (1999) POLYRATE, Program vision 8.2, Minneapolis
47. Calandra P, Longo A, Ruggirello A, Liveri VT (2004) J Phys Chem B 108:8260–8268
48. Carlo SR, Torres J, Fairbrother DH (2001) J Phys Chem B 105:6148–6157